Journal of Energy Chemistry 26 (2017) 284–294

Contents lists available at ScienceDirect

Journal of Energy Chemistry

journal homepage: www.elsevier.com/locate/jechem

http://www.journals.elsevier.com/journal-of-energy-chemistry/

Analysis of the factors controlling performances of Au-modified TiO_2 nanotube array based photoanode in photo-electrocatalytic (PECa) cells

Claudio Ampelli[a,*], Francesco Tavella[a], Chiara Genovese[a], Siglinda Perathoner[a], Marco Favaro[b,1], Gabriele Centi[c]

[a] Department of Chemical, Biological, Pharmaceutical and Environmental Sciences, University of Messina, ERIC aisbl and CASPE/INSTM, V.le F. Stagno d'Alcontres 31, 98166 Messina, Italy
[b] Department of Chemical Sciences, University of Padua, via Marzolo 1, 35136 Padua, Italy
[c] Department of Mathematical, Computer, Physical and Earth Sciences, University of Messina, ERIC aisbl and CASPE/INSTM, V.le F. Stagno d'Alcontres 31, 98166 Messina, Italy

ARTICLE INFO

Article history:
Received 6 July 2016
Revised 31 August 2016
Accepted 18 October 2016
Available online 15 November 2016

Keywords:
H_2 production
Au nanoparticles
Solar fuels
TiO_2 nanotubes
Electrodeposition
Photoelectrochemical cells (PEC)
Solar-to-hydrogen efficiency
Anodic oxidation

ABSTRACT

The efficiency of photo-electrocatalytic (PECa) devices for the production of solar fuels depends on several limiting factors such as light harvesting, charge recombination and mass transport diffusion. We analyse here how they influence the performances in PECa cells having a photo-anode based on Au-modified TiO_2 nanotube (TNT) arrays, with the aim of developing design criteria to optimize the photo-anode and the PECa cell configuration for water photo-electrolysis (splitting) and ethanol photo-reforming processes. The TNT samples were prepared by controlled anodic oxidation of Ti foils and then decorated with gold nanoparticles using different techniques to enhance the visible light response through heterojunction and plasmonic effects. The activity tests were made in a gas-phase reactor, as well as in a PECa cell without applied bias. Results were analysed in terms of photo-generated current, H_2 production rate and photo-conversion efficiency. Particularly, a solar-to-hydrogen efficiency of 0.83% and a Faradaic efficiency of 91% were obtained without adding sacrificial reagents.

1. Introduction

The photo-electrocatalytic (PECa) approach for solar fuel generation is an emerging technology for the future of sustainable energy [1–3]. There is a clear trend to develop alternative solutions to the use of fossil fuels, with solar fuel/chemicals production being a key factor to enable this transition to a new resource and efficient production of energy [4]. PECa solar cells, e.g., cells with separated zones for the reactions of oxidation and reactions necessary to produce solar fuels, are a critical technology to realize this objective [5–7]. Although different configurations exist for this type of cells [6,7], the most common cell is based on a semiconductor photo-anode where water is oxidized to O_2 and H^+/e^- with the latter transported to the other half-cell of the PECa device to either produce H_2 (in a compartment different from that of oxygen evolution, an important factor for device exploitability and security of operation) or reduce CO_2. While most of the literature studies are based on operations of both the electrodes (for water oxidation and H_2 production or CO_2 reduction) in the presence of a liquid bulk electrolyte [7], we have earlier shown how the operations in electrolyte-less conditions (gas-phase type electrodes, similar to the gas-diffusion layer – GDL – electrodes used in PEM-type fuel cells) may be advantageous for various reasons. This type of PECa cell design [6,8] also requires different characteristics for the photo-anode [8,9] with respect to those operating in the presence of an electrolyte. In particular, a specific type of nanostructure, as that based on an array of vertically-aligned semiconductor nanotubes, is necessary for an efficient transport/collection of both photo-generated electrons and protons during the water oxidation [9].

Therefore, in addition to the general issue of developing improved photo-active materials for water oxidation, there are specific design issues related to the development of advanced photo-anodes for the type of PECa cells discussed above. The latter

* Corresponding author.
E-mail address: ampellic@unime.it (C. Ampelli).
[1] Present address: Advanced Light Source, Joint Center for Artificial Photosynthesis, Lawrence Berkeley National Laboratory, 1 Cyclotron Rd., M/S 30R0205 Berkeley, CA 94720, USA.

http://dx.doi.org/10.1016/j.jechem.2016.11.004

aspects have been in general much less addressed and there is the need of a better understanding of the factors controlling the performances in this type of photo-anodes, which is the scope of the present work.

Among the many recent papers about photo-electrodes for water splitting, it may be cited, for example, the works of Zhou and Xie [10] on the development of new photo-active materials and their characterization in terms of UV–visible light absorption, band gap and quantum yield; Russo et al. [11] on $BiVO_4$; Natali Sora et al. on $LaFeO_3$ [12]. Moreover, Lhermitte and Bartlett [13] reviewed the use of $CuWO_4$ electrodes for water oxidation, Kang et al. [14], the synthesis and properties of different photoelectrodes for water splitting, Yang et al. [15], the use of earth abundant materials for the use in PECa devices for water splitting, and Domen and coworkers [16] the recent advances in semiconductors for water splitting. It may be remarked that, in general, the preparation of these materials is often not related to the type of electrochemical device utilized, or that the form in which these materials are developed is not well suitable for the type of PECa cell (electrolyte-less) discussed above [17]. We may also note that from a practical point of view, it would be preferable to evaluate the total productivity of the cell than the properties of the single catalytic materials or their photocatalytic activity in the degradation of organic dyes and pollutants [18–20].

From this perspective, electrochemistry and electrochemical engineering assume an important role in the development of the future technologies in energy chemistry [21,22]. In our previous papers, we also showed that synthesis of the materials (for the preparation of the electrodes) and design of the cell (in terms of reactor configuration and operating conditions) are both of extreme importance for the development of highly-efficient PECa devices for solar fuel generation [23,24]. Mass transport limitations and charge recombination phenomena are the main issues that strongly limit performance of PECa cells, especially for the electrochemical reduction of CO_2 [25,26].

Performance and stability of PECa cells are largely determined by the processes occurring at the interface with the electrode; hence, the electrode structure (i.e., the development of 2D or 3D nanostructured electrodes) is one of the key factor to increase the efficiency of solar PECa cells. Recently, Xu et al. [27] proposed the construction of photonic nano systems based on 3D porous reduced graphene oxide (RGO) and TiO_2 aerogel for solar water splitting. They presented a good example of fabrication of three-dimensional porous photo electrodes, which are necessary to ensure high active surface area and promote light trapping, charge separation and transport. Moreover, the simulation of transport phenomena in PECa reactors may help in designing properly the reactor configuration, to attain the maximum benefits from the irradiation patterns and minimize the high overpotentials typically encountered in such kinds of cell. The use of plasmonic enhancement for solar water splitting, in general, is an area of fast growing relevance [28–30].

These studies usually take into account the transport phenomena equations (Navier–Stokes equations), the energy equation for the electrolyte and the radiative transfer equation, providing useful information about the suitable reactor design for enhancing solar-to-hydrogen efficiency and hydrogen production. However, quite a few studies have investigated the PECa reactor design [31–33] and they are mainly focused on heat transfer and flow characteristics without taking into account the influence of the electrode structure and porosity on the efficiency of PECa cells.

This contribution would like to stress the importance of a multidisciplinary approach for the development of solar PECa cells by considering: (i) the chemistry of the materials, which is the base for the synthesis of suited photo- and electro-catalysts to be assembled and implemented for the fabrication of nanostructured electrodes (by a nanoscale engineering approach); and (ii) the engineering of the device, for maximizing the overall solar energy conversion performance. Particularly, the discussion will be made by evaluating the critical factors controlling PECa performance, through the analysis of the results obtained from experimental tests on plasmonic-type photo-anodes based on Au-modified TiO_2 nanotube arrays. These nanostructured electrodes were irradiated by a solar simulator within a novel PECa device [6,8] and tested in the processes of both water photo-electrolysis and ethanol photo-dehydrogenation for the production of hydrogen.

The evaluation of the factors influencing the behaviour of solar PECa devices evidences the need of approaching in multidisciplinary way, including: (i) nano-engineering for designing the electrodes; (ii) catalysis and reaction engineering and (iii) industrial engineering, to attain the maximum benefits from the cell configuration for a real industrial implementation.

Vertically aligned TiO_2 nanotubes were prepared by controlled anodic oxidation of Ti foils. It is an already consolidated technique [34–36], easily scalable, for the formation of highly ordered TiO_2 nanotube arrays, although the correlation of the characteristics of these titania nanostructured thin films with the relevant properties for PECa devices, such as (i) enhanced visible light absorption and (ii) improved charge separation characteristics, are less investigated [37,38].

With the aim to further enhance the visible response by heterojunction and plasmonic-type effects, gold nanoparticles (Au NPs) were also deposited on the TiO_2 nanotubes using different techniques. In addition to the commonly-used wet impregnation and photo-deposition techniques, we also present here a modified electrodeposition technique for Au NPs, based on multiple cycles of voltage ramps followed by a selective washing treatment. This method aims at controlling the nucleation phase of Au NP formation, limiting their aggregation and removing the excess of Au that weekly interacts with the TiO_2 surface. The motivation to investigate different methods of deposition is related to the great role of the size and dispersion of Au NPs, as well as their interaction with the semiconductor, to determine the H_2 productivity and efficiency of the PECa cell.

Although we focus discussion here on the formation of H_2 in PECa cells, the same type of devices, but with tuned type of electrocatalysts, may be used also for the reduction of CO_2 as reported elsewhere [39–41].

2. Experimental

2.1. Preparation of TiO_2 nanotube arrays

TiO_2 nanotube (TNT) photo-electrodes were prepared by controlled anodic oxidation of Ti foils. The essence of the method can be described as a reconstruction of a thin TiO_2 layer (formed initially by oxidation of a Ti foil) which occurs under the application of a constant voltage in the presence of fluoride-based electrolytes [34–36]. The starting titanium disc (Alfa Aesar, 0.025 mm of thickness, 3.5 cm of diameter) was anodized using a two-electrode electrochemical cell working at room temperature at 50 V. The reaction bath consisted of a solution of ethylene glycol with H_2O (2 wt%) and NaF (0.3 wt%). The set voltage was gradually reached by a programmed ramp at 3 V/min and then kept constant for the whole anodization (5 h). Details about the geometry of the cell and procedure of preparation were described elsewhere [24,42]. After the preparation, the nano-structured amorphous substrates were annealed at 450 °C in air for 3 h in order to induce crystallization into the anatase phase. A thin Ti layer remained non-oxidized, thus acting as an electron-collective layer during the photo-catalytic process.

2.2. Deposition of Au

Three techniques were investigated for the decoration of TNT with Au NPs: (i) wet impregnation, (ii) photo-reduction and (iii) electrodeposition.

A typical wet impregnation technique was adapted for the deposition of gold on a substrate in the form of a thin film instead of a powder. The as-prepared TNT/Ti film (after calcination) was located at the bottom of a decanter (having about the same size of the round TNT/Ti film), which was filled with an aqueous solution of $HAuCl_4$ and heated at 60 °C under constant slow stirring until complete evaporation of water was achieved.

The photo-reduction method was carried out in gas phase: the as-prepared TNT/Ti film was first immersed into the metal precursor aqueous solution ($HAuCl_4$) for 30 min, allowing the nanotubes to fill in by the capillary forces. Then, it was exposed to an UV–visible lamp under a low inert gas flow to form the NPs in a photo-reduction process. The lamp was the same utilized for the irradiation of the PEC cell (see below in paragraph 2.4).

Electrodeposition technique was performed in a conventional electrochemical cell with a three-electrode configuration using Ag/AgCl as the reference electrode and a Pt rod as the counter-electrode. The as-prepared TNT/Ti film (acting as the working electrode) was subjected to cyclic voltammetry in presence of the metal precursor ($HAuCl_4$) in 1 M phosphate buffer solution (PBS). In particular, seven cycles from 0 to + 1.4 V (and reverse) were performed at a scan rate of 20 mV/s and 50 °C temperature. Finally, the excess of Au was removed by washing with deionized water in an ultrasonic bath (2 min).

After depositing gold on TiO_2 using one of these three techniques, the TNT/Ti film was dried in air at 200 °C for 2 h with a heating rate of 2 °C/min.

2.3. Characterization

The structural and morphological characterization of the materials was made by scanning electron microscopy (SEM) with high resolution field emission gun (Zeiss SUPRA 35 VP), operated at a primary beam acceleration voltages of 5 kV, equipped with an energy-dispersive X-ray (EDX) analyzer. The oxide layer sizes (nanotube diameter and length) were directly obtained from SEM images. Ultraviolet–visible diffuse reflectance spectra were recorded by a Jasco V570 spectrometer equipped with an integrating sphere for solid samples, using $BaSO_4$ as reference and in air. Chronoamperometry measurements were performed by the use of a three-electrode photo-electrochemical cell, with a Pt wire as counter-electrode and a saturated KCl-Ag/AgCl reference electrode. All the tests were performed at room temperature in 1 M KOH solution at 0.1 V using a 2049 AMEL potentiostat–galvanostat. Atomic absorption spectroscopy (AAS - AAnalyst 200 Perkin Elmer) was used to determine the effective gold loading, after dispersion of the samples in an aqueous HF solution in ultrasonic bath. The phase composition and the degree of crystallinity were analysed by X-ray diffraction analysis with an ADP 2000 diffractometer using a Cu-$K\alpha$ radiation. Data were collected at a scanning rate of 0.025/s in a 2θ range from 20 to 80°. Diffraction peak identification was made on the basis of the JCPDS database of reference compounds.

2.4. Gas-phase reactor and PECa device

The experimental apparatus for the photo-(electro) catalytic experiments consists of a solar illuminator, a photo-reactor and a gas chromatograph for the analysis of products.

The solar illuminator is a Xe-arc lamp (Lot Oriel, 300 W) equipped with a set of lenses for light collection and focusing, a water filter to eliminate the infrared radiation and a set of filters to select the desired wavelength region, thus evaluating the photo-response in ultraviolet or visible regions.

The Au-modified TiO_2 nanotube arrays were studied in two reactions: (1) the photo-production of H_2 in the presence of an alcohol and (2) the water photo-electrolysis (splitting). For the first reaction, a gas-phase photo-reactor (GPR) was used, while a PECa type cell was used in the second case.

The GPR is made of Pyrex and equipped with a quartz window that allows irradiating a photocatalytic area of ~10 cm^2. The photocatalytic substrate, prepared as a thin film, was suspended within the reactor headspace and irradiated perpendicularly by light coming from the external lamp. An aqueous ethanol solution, having a controlled temperature (60 °C) and composition (10 vol%), was present on the bottom of the reactor maintaining the gas in equilibrium with the liquid phase. Details about the GPR were reported elsewhere [43,44].

The PECa reactor is made of Plexiglas and equipped with a quartz window. It has a two-electrode configuration with two separate compartments for the reduction and oxidation half-reactions. The irradiated area is ~10 cm^2. 1 M NaOH aqueous solution was used as electrolyte in the anodic compartment, while 0.5 M H_2SO_4 aqueous solution was used in the cathodic side of the PECa cell. The principle of working of the PECa device can be summarized as follows: (i) light irradiation induces a charge separation (electrons and holes) on the Au/TiO_2 surface (photo-anode) where the holes oxidizes the water to O_2; (ii) the protons pass through a Nafion® membrane to the other compartment (cathode), while the electrons, collected by the Ti layer, reach the cathode through an external wire and (iii) the protons recombine with the electrons on the electrocatalyst surface (commercial Pt supported on carbon cloth, by E-TEK®) to give H_2. Before its use, the Nafion® membrane was treated with H_2O_2 to remove organic impurities and then in H_2SO_4 for activation. A potentiostat–galvanostat (AMEL 2049) interfaced with a Personal Computer, was used to measure the photo-generated current. Details about the assembling of the working electrode were reported elsewhere [24,45].

A gas chromatograph (GC) with a thermal conductivity detector (TCD) was used to analyse the permanent gases (H_2, O_2, CH_4 and CO) by a molecular sieve column (5A Plot). Carbon dioxide, ethanol and acetaldehyde were instead analysed by a fused silica column (Rt-Qbond).

3. Results and discussion

3.1. TNT characterization

Highly ordered vertically aligned TiO_2 nanotubes (TNT) were prepared by controlled anodic oxidation, as reported in the experimental part. The peculiarity of this technique lies in its capability to tailor the desired nano-architecture by modulating the synthetic parameters during the anodization, such as the applied voltage, the time of anodization, the nature of the electrolyte, the quantity of H_2O, the pH.

Fig. 1 shows some SEM top images of TNT arrays prepared at 50 V. After the preparation the surface of the photo-layer was partially covered by amorphous oxide (Fig. 1a), which limits its photo-response. The debris can easy be removed by short etching with concentrated HCl (30 s) in ultrasonic bath; Fig. 1(b) shows the clean TNT surface after the sonication treatment, which is of fundamental importance to enhance light harvesting and photocatalytic activity. The inset of Fig. 1(b) shows a magnification of the top surface of TNT, evidencing an average inner diameter of ~70 nm and a wall thickness of ~8–10 nm. The thickness of the oxide (which corresponds to the length of the nanotubes) was measured as ~1.2 μm. This is an average value because the sonication treatment creates slightly differences at microscale. The growth of

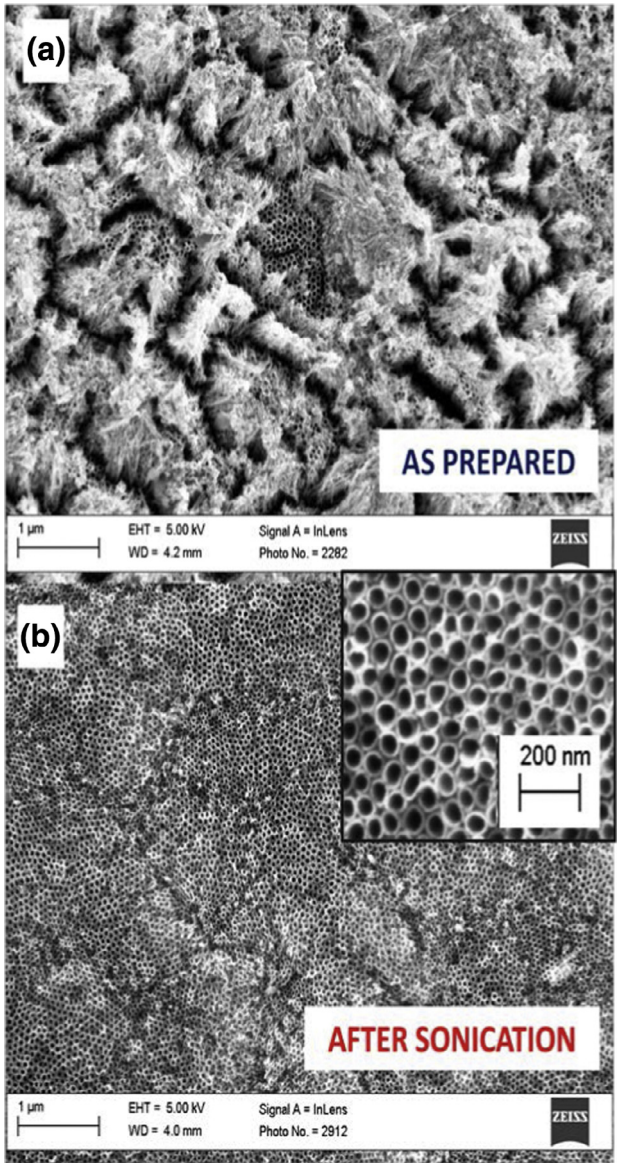

Fig. 1. SEM top images of (a) the as-prepared TiO_2 nanotube arrays anodized at 50 V and (b) the same nanotubes after sonication treatment. The inset shows a magnification of the cleaned top surface.

the nanotubes is the result of the equilibrium between two reactions: (i) the controlled oxidation of Ti, due to the application of a strong electromagnetic field and (ii) the partial dissolution of the oxide, due to the presence of fluoride anions in the reaction bath.

The length of the nanotubes has much influence on performance of a PECa cell, as the transport of electrons occurs from the top of the nanotubes, where light harvesting is the greatest, to the bottom of the nanotubes and towards the collector layer (which is the metallic Ti remained non-oxidized after the anodization). Light absorption could be maximized by increasing the quantity of the photo-catalytic materials, i.e., obtaining longer TNT by increasing time of anodization. However, we have demonstrated that, in PECa cells, the longer TiO_2 nanotubes are the more charge recombination phenomena occur; thus, a thin nanotube layer is preferable. The only feasible engineering solutions to increase light harvesting (not considering the nature of the photo-catalytic material) refer to: (i) increase the irradiated surface area, (ii) create an ordered nano-architecture (and 3D porosity) in the photo-catalyst, (iii) diminish light scattering phenomena and (iv) clean the surface from not-absorbing (nano) objects. The relationship between thickness of the photo-layer and PEC performance was deeply studied and reported elsewhere [46].

The nanometer-sized Au NPs are known to exert visible-light absorption, a phenomenon that is due to the surface plasmon resonance (SPR) [47]. The morphologies of the prepared vertically aligned Au-modified TNT arrays are shown in Fig. 2.

Wet impregnation resulted preferentially in samples showing aggregation of not well-dispersed Au NPs and deposited mainly on the top of the TNTs (Fig. 2a). Photo-reduction method has been reported in literature as a more suitable technique for obtaining very small NPs [48]. In our case, even if smaller and quite dispersed NPs were obtained with respect to wet impregnation method (8–15 nm), some debris was present on the TiO_2 surface, which are residuals from the evaporation of the aqueous solution containing the precursor salt (Fig. 2b).

Electrodeposition seems to be the best method for decorating homogeneously the surface of the TNTs. Fig. 2(c) shows a top view of the TNT arrays obtained using this technique. The dispersion of the Au NPs is more uniform with respect to the sample prepared by wet impregnation and comparable with the sample obtained by photo-reduction. However, very small Au NPs (3–5 nm) can be observed preferentially on the top of TNTs, in correspondence with the edges of the tubes (Fig. 2c). EDX analysis confirmed the presence of gold on the TNT surface. A few bigger Au NPs (with size similar to the opening of the tubes) blocked up the holes of some tubes in spite of the post-sonication treatment to remove the excess of Au. The major part of Au NPs was deposited on the top of TNTs, due to the resistance encountered by the aqueous Au precursor solution to fill completely the tubes by capillarity.

Fig. 3 reports the UV–visible diffuse reflectance spectra of the Au-modified TNT arrays prepared according with the three studied modalities of Au deposition. The spectra of the bare TNT arrays (non-modified) and commercial TiO_2 P25 Degussa (for reference) have also been reported.

All the spectra exhibit a strong absorption band centred at about 350–400 nm related to the lowest energy charge transfer $O^{2-} \rightarrow Ti^{4+}$ and thus associated to the TiO_2 band gap consistent with expectations for a mixture of *anatase* and *rutile* TiO_2 polymorphs. TNT modification by gold shifts the band gap up from 3.3 eV to about 3.1 eV depending on the method of deposition (see table in Fig. 3). It should be observed that TiO_2 P25 Degussa has a band gap shifted to lower frequencies with respect to the TNT arrays, due to the presence of about 20 wt% of *rutile* phase in the P25 sample, while TNT arrays show only *anatase* phase, as discussed below.

Except for TiO_2 P25 Degussa, all the spectra also evidence a broad absorption peak centred around 550 nm, with a broad tail on the low energy side extending to the whole visible region. Note that the apparent series of peaks above about 550 nm for the Au-modified TNTs by electrodeposition is due to light diffraction interferences.

It may be noted that non-modified TNT sample shows also a broad absorption band in the visible region, although with a maximum centred around 650–700 nm. This absorption band is not present in films of TiO_2 prepared by sol–gel or by depositing commercial TiO_2 nanoparticles (such as P25). It is related to light diffraction in 2D-type photonic materials [49,50]. TNT arrays show a periodicity of the crystal structure that is in wavelength equal to 600–750 nm. The result is an improvement in terms of visible light harvesting, although it must be noted that this strong visible-light absorption (being related to light diffraction, rather that absorption with generation of charge separation) does not produce in principle an improved photocatalytic activity.

In photonic crystals, due to the periodically structured electromagnetic medium, light cannot propagate through the structure

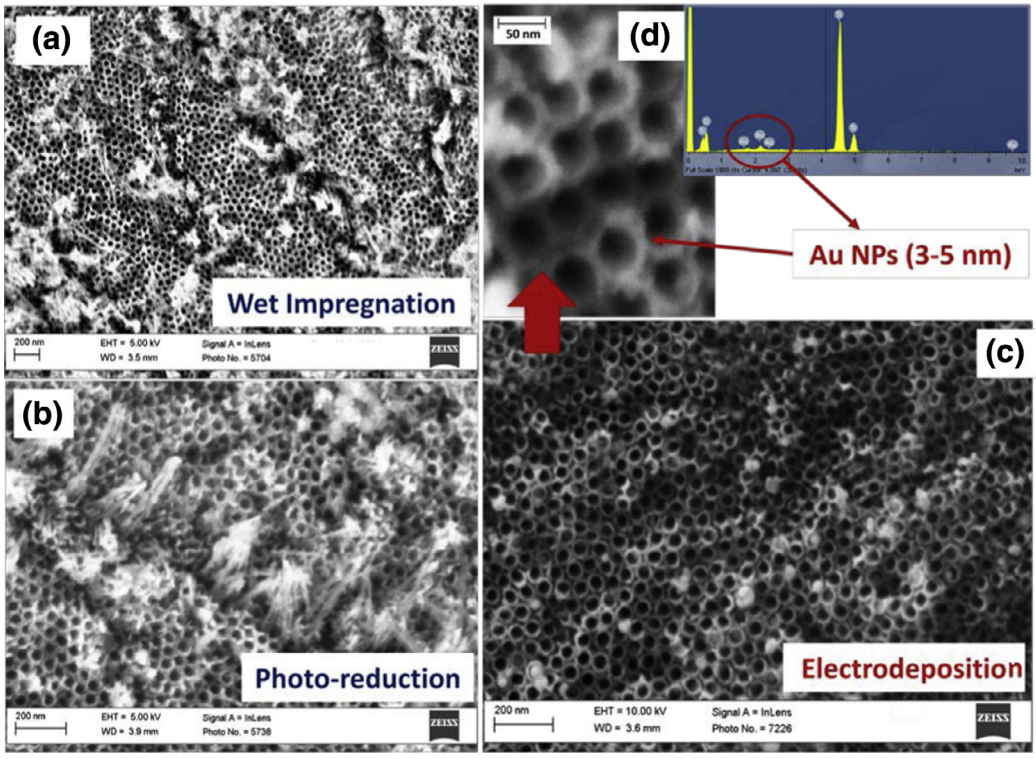

Fig. 2. SEM top images of Au-modified TNT arrays with Au deposited by (a) wet impregnation, (b) photo-reduction, (c) electrodeposition. In (d) a magnification of (c) image is reported showing 3–5 nm Au NPs. EDX analysis is also reported.

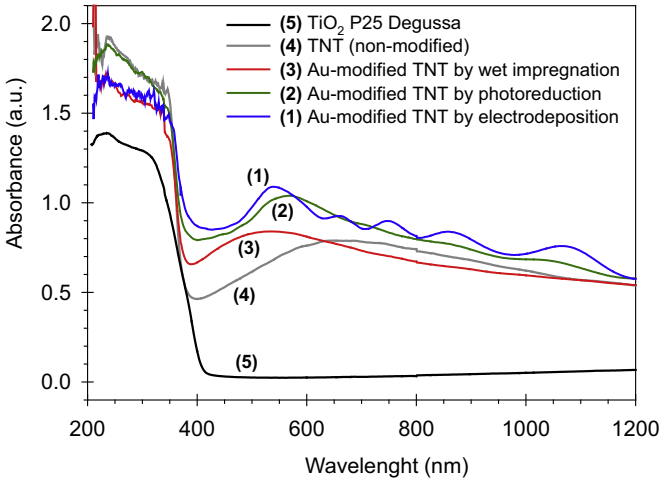

Photo-anode	Band gap (eV)
TNT	3.26
Au-modified TNT by wet impregnation	3.16
Au-modified TNT by photo-reduction	3.13
Au-modified TNT by electrodeposition	3.08
TiO_2 P25 Degussa	3.04

Fig. 3. UV–visible diffuse reflectance spectra of Au-modified TNT arrays prepared by different Au deposition methods. The table in the figure reported the calculated band gaps.

and thus is localized and trapped, creating an intense local electromagnetic field which may interact with other incoming photons, allowing the generation of some hot-electrons (injected into the valence band of the semiconductor) [51]. The mechanism, although less efficient, is similar to that present in plasmonic materials (for example, gold NPs deposited on TiO_2), where two mechanisms of hot-electron generation exist [52–54]: (i) plasmon-induced resonant energy transfer and (ii) direct electron transfer. The first consists in the non-radiative dipole–dipole coupling between the plasmon of the metal and the electron-hole pairs in the semiconductor. The second, typically referred to as "hot" electron injection, involves the transfer of plasmonic electrons over the interfacial Schottky barrier established between the Fermi level of the metal and the conduction band of the semiconductor. Metals with a larger density of electronic states, as in the case of the d-band electrons in Au, are necessary for an efficient mechanism. The strong localized electromagnetic field created by a photonic nanostructure of the semiconductor, such as in our TNT system, may positively further interact with this mechanism of visible-light generation of charge separation in wide-band gap semiconductors (such as TiO_2). Therefore, it is possible to develop visible light responsive TiO_2-based photoelectrodes based on the synergetic interaction between Au-based plasmonic responses and TiO_2 photonic crystals [51].

In Fig. 3, it is evident that the deposition of Au NPs on TNT arrays slightly intensifies and shifts to wavelengths below 600 nm the maximum in the broad absorption band, although the specific effect is largely depending on the method of Au NP deposition. The presence of interference fringes in the range 600–1200 nm in the spectrum of Au-modified TNT arrays prepared by electrodeposition is probably related to the difference in localization of Au NPs with respect to the other two methods of preparation, as discussed before. Likely, very small Au NPs on the top of the TNTs induce a localized surface resonance coupling with the resonances deriving from the Au NPs localized in other positions of the TNTs, where they are more influenced from the electromagnetic field generated by the photonic crystal. This could explain the interference fringes observed in this sample, differently from the other samples (Fig. 3), although more studies are necessary to better clarify this effect. This interpretation, however, supports the idea of the

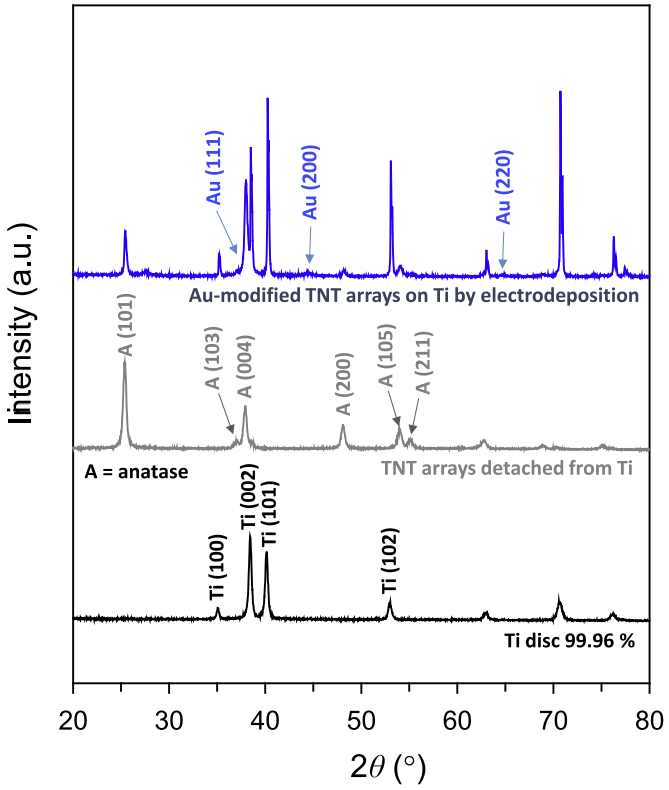

Fig. 4. XRD patterns of (i) Au-modified TNT arrays on Ti with Au deposited by electrodeposition, (ii) TNT arrays detached from the Ti layer and (iii) pure Ti disc (99.96%).

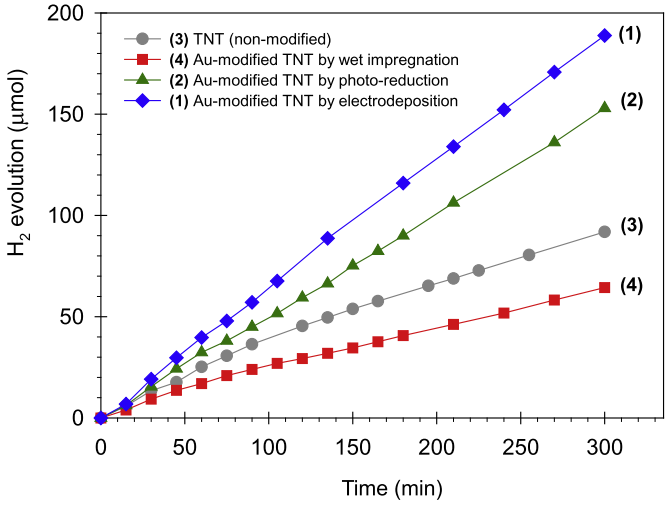

Fig. 5. Hydrogen evolution as a function of time in gas-phase photo-catalytic experiments of ethanol photo-dehydrogenation over Au-modified TNT arrays.

coupling between photonic and plasmonic effects in Au NPs/TNT systems, and that this effect greatly depends on the characteristics (related to the method of gold deposition) of the Au NPs. Cai et al. [55], studying the photo-catalytic activity of 3D ordered macroporous gold-loaded TiO_2 photonic crystals, observed the same interference fringes with similar frequency for the Au-TiO_2 sample with lower Au loading (1 wt%). This sample also showed the lowest Au NP size (about 6 nm), even if the ordered TiO_2 structure was different with respect to our TNT arrays. They also found that, by incorporating Au NPs in TiO_2 films, the lifetimes of the UV–visible excited electrons and holes are extended, limiting the charge separation phenomena.

TNT arrays prepared by anodic oxidation show a BET surface area slightly higher than Degussa P25 (68.1 vs. 48 m^2/g) and no significant changes were observed after Au deposition. The phase composition was investigated by XRD and the obtained patterns are shown in Fig. 4.

As already reported in the experimental part, the TNT arrays are amorphous after the anodization, thus the samples were annealed to induce crystallization. The XRD pattern for TNT/Ti sample showed a 100% *anatase* structure (no *rutile* phase was detected in all the samples, expect for TiO_2 P25 Degussa). To discern the peaks related to anatase (A) TiO_2 from the Ti peaks, the TNT arrays were completely removed by a strong sonication treatment and then analysed by XRD; results are also reported in Fig. 4, together with the pattern obtained for the only Ti support.

Diffraction Au peaks (as reported in the JCPDS file No. 04-0784) were also observed, even if barely discernible from the background, due to the low Au concentration on TNT and to the small size of Au NPs obtained by electrodeposition technique, as confirmed by SEM analysis. To evaluate the effective Au metal loading in TNT, the as-prepared Au-modified TNT arrays were sonicated in concentrated HF aqueous solution (48 wt%) to dissolve Au and the resulting solutions, after proper dilution, were analysed by AAS. Calibration curves were obtained by means of three standard solutions in the range 1–5 ppm by diluting gold atomic spectroscopy standard concentrate (1.00 g/L) supplied by Sigma Aldrich. The analytical results showed ~1.5 wt% Au loading for the sample prepared by electrodeposition; a similar value was detected for the Au-modified TNT sample prepared by photo-reduction, while the Au loading for the sample prepared by wet impregnation was higher (2.4 wt%).

3.2. H_2 production

Fig. 5 shows the H_2 formation activity in gas-phase experiments of the different Au-modified TNT arrays. A maximum in productivity to hydrogen was observed for the photo-catalyst prepared by electrodeposition, giving about 190 μmol H_2 in 5 h of light irradiation. For the sample with Au deposited by photo-reduction technique, H_2 evolution was about 19% lower. While the effective Au loading is similar, the higher performance for Au-modified TNT arrays by electrodeposition should be ascribed to the smaller Au NPs obtained using this Au deposition technique, as confirmed by SEM analysis. As commented regarding Fig. 3, however, the sample prepared by electrodeposition shows also a better effective interaction between plasmonic and photonic effects to enhance interaction with the light. This is a likely alternative interpretation of the enhanced photocatalytic activity in H_2 generation. Hydrogen evolution for the sample prepared by wet impregnation was even less than the non-modified TNT arrays. In this sample, no small Au NPs are present on the top of the TNTs and Au aggregates are partially covering the photo-active surface. Although in principle the latter effect may reduce performance with respect to bare TiO_2, it is likely that trapping of electrons by large metal particles may enhance in this case charge recombination and thus a lowering of performance. This result well indicates that simple addition of gold particles may result in lower performances, in the absence of specific characteristics in which these NPs enhance the photocatalytic behaviour, for example through the effective plasmonic–photonic interaction, as commented above.

As reported in the experimental part (paragraph 2.4), these experiments were performed by using a GPR reactor in the process of ethanol photo-dehydrogenation/reforming. The main side product was acetaldehyde, evidencing that dehydrogenation process prevails over the reaction of complete ethanol reforming to give CO_2. Although formally these are photocatalytic tests, we believe that may more correctly be described as a short-circuit-type

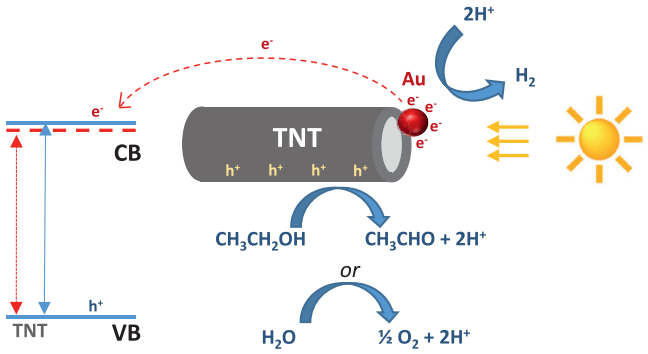

Fig. 6. Schematic mechanism of water photo-electrolysis and/or ethanol photo-dehydrogenation over Au-modified TNT arrays with both redox reactions occurring in the same environment.

electrochemical cell, with the TNT arrays being the anode for the oxidation reaction and the Au NPs the cathode for the proton reduction. The holes created in TNTs during light irradiation, oxidize ethanol to acetaldehyde (and/or water to O_2), while electrons are attracted by Au NPs combining with protons coming from the ethanol deprotonation. This tentative mechanism is depicted in Fig. 6.

Jana et al. [56], in studying the photoelectrochemical behaviour of Au NPs on TNT substrates, pointed out the critical role of the electrode–electrolyte interface in plasmonic generation of free charges on the NP surface. Charge separation occurred by the transfer of photo-excited electrons from the Au NPs to TNT conduction band and simultaneous transfer of compensative electrons from a donor in solution to the Au NPs. They also reported that Au NPs and TNTs form a Schottky junction, which is the reason of band bending at their interfaces. The result is a reduced recombination of photogenerated electrons and holes in the junction region (heterojunction effect) and more charge carriers available for the redox reactions. It may be remarked that in our experiments (Fig. 5), we operate in the absence of an electrolyte, in the gas-phase type reactor described in the experimental part. The Au NPs/TNT photocatalyst is thus in contact with the gas phase where ethanol and water are present at the equilibrium with the liquid solution present at the bottom of the reactor (not in direct contact with the photocatalysts). The explanation of Jana et al. [56] about the role of the electrolyte in the process may thus be not applied correctly, although it is evident from the data reported in Fig. 5 that a linearity in H_2 generation is present. The redox processes are reasonably closed by the conducting properties of the semiconductor (TNT) and the surface mobility of charged species (like protons). Likely, these are the limiting factors in performances in our gas-phase approach, even if there are other potential advantages in terms of reduced light scattering, gas cap, formation of double layer and associated mass transfer limitations, etc. [6,8]. By a better design of the semiconductor properties (improving hydrophilicity, for example) and electrode engineering (some aspects discussed below), in addition to a proper design of the Au NPs/TNT materials to exploit better the phononic–plasmonic interaction, it is likely possible to improve the performances of these photocatalysts in H_2 generation.

It may also be observed that within the lab-scale time range investigated (up to about 20 h) there is no deactivation of the catalysts, especially in the more active ones (some deactivation is observed in bare TNTs and Au-modified TNTs prepared by wet impregnation, as shown in Fig. 5). This suggests that there is no relevant adsorption and surface polymerization of the acetaldehyde formed as a main production in ethanol dehydrogenation.

Selectivity of the reaction to acetaldehyde is rather high, above 98% and thus this reaction, which may likely be extended to other types of alcohols or possible other types of substrates, can be a good example of solar-driven chemistry, e.g., a type of chemistry based on the direct use of solar energy or more in general renewable type of energy. From a sustainability perspective, waste streams containing ethanol can be converted selectively to H_2 and acetaldehyde (both valuable chemicals) without the formal need to supply energy, except solar one. This evidences the interest in this type of solar-driven catalytic chemistry. It may also be noted that even if the superhydrophilic behaviour of TiO_2 upon irradiation is well known, and thus the dehydration of ethanol (formation of ethylene) may be expected to be relevant, this reaction is minimized in our Au NPs/TNT photocatalysts. There is likely a role of the specific TiO_2 nanostructure on this peculiar behaviour, although to be investigated more in detail.

3.3. PEC performance

Performance of a PECa cell is determined by the ability of a photo-electrode to carry out the following processes: (i) light harvesting, (ii) generation of electric charge carriers, (iii) carrier migration towards the interface between photo-electrode and electrolyte and (iv) carrier transportation towards the external circuit to the place where hydrogen formation occurs [57].

Being a solar simulator utilized in our apparatus for measuring the PECa cell performances, the first requirement is to measure the irradiance of the lamp. A spectroradiometer system (Lot Oriel, model ILT950) was used for this purpose. Particularly, the probe connected to the spectroradiometer by means of optical fibre was located within the reactor replacing the photo-active material. The measured irradiance was 135 mW/cm^2, which represents the light energy reaching the Au-modified TNT arrays when irradiated by the solar illuminator. In order to evaluate the real light absorbance from the photo-active material, the TNT layer was detached from the metallic Ti (remained not oxidized after the anodization) and the probe was located behind the obtained transparent TNT membrane, thus measuring the light transmittance. The resulting value in terms of irradiance was 59 mW/cm^2, which represents the effective quantity of light absorbed by the photo-anode.

The samples were then exposed to light irradiation for chrono-amperometric measurements, using different filters to select the desired wavelength region. Fig. 7(a) shows the typical photocurrent vs. time profiles referred to non-modified TNT arrays, obtained in a three-electrode cell using an aqueous solution of 1 M KOH at 0.1 V (Ag/AgCl reference electrode, Pt counter-electrode).

The ON/OFF illumination at open spectrum displayed a quick rise in photocurrent and fast recovery to the original value through multiple ON/OFF cycles (four cycles). There is a stable and reproducible photocurrent for all the tested samples. By using the AM 1.5 G filter (simulating standard terrestrial solar irradiance distribution) the ON/OFF increment was ~18% with respect to the value at open spectrum (no filter). Considering that the percentage of UV light in solar spectrum is only 4%, this result obtained by AM 1.5 G filter evidences the improved performance of TNT arrays in the visible region with respect to standard TiO_2 (active only when irradiated by ultraviolet light, see UV–visible spectrum in Fig. 3). This is related to the effect previously discussed with reference to the results reported in Fig. 3. Fig. 7(b) shows the TNT photocurrent profile in comparison with data obtained by irradiating the Au-modified TNT arrays with gold deposited by the three different deposition techniques.

Electrodeposition method allows enhancing the photocurrent response, being 1.6 times higher than the photocurrent of the non-modified TNT arrays, which becomes 1.8 times higher when the AM 1.5 G filter was used. The other two gold deposition techniques

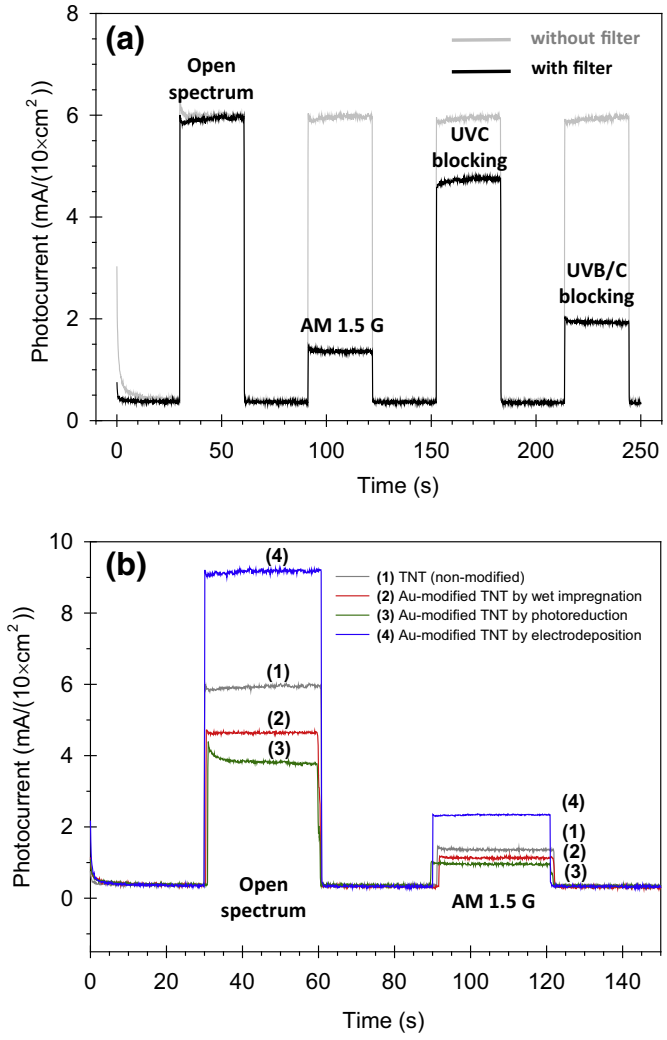

Fig. 7. Chronoamperometric measurements for (a) non-modified and (b) Au-modified TNT arrays (0.1 V, 1 M KOH).

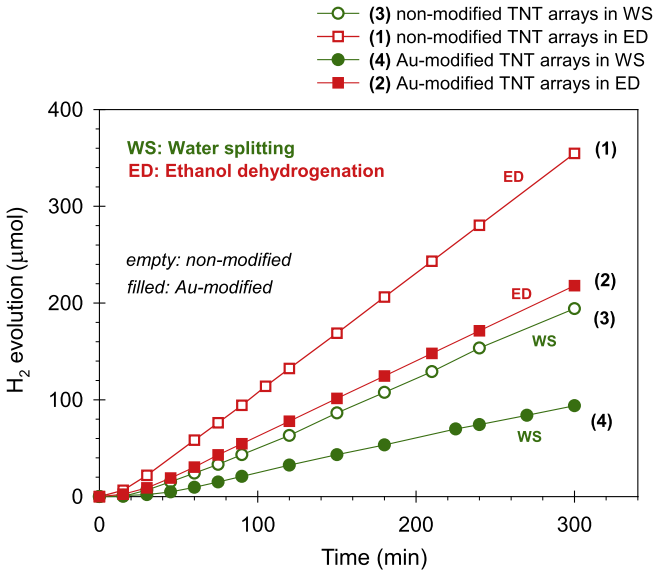

Fig. 8. Hydrogen evolution as a function of time from the cathode of a PECa cell in water splitting (WS) and ethanol dehydrogenation (ED).

(wet impregnation and photo-reduction) do not give any improvements and photocurrent values even diminished with respect to the non-modified sample. There is a good correlation between activity in H_2 generation (Fig. 3) and photocurrent generated (Fig. 7), confirming the close link between the two effects.

The best Au-modified TNT film (obtained by electrodeposition) was then tested in the PECa reactor in H_2 production by both water splitting and ethanol photo-dehydrogenation. The non-modified TNT arrays were used as reference in these tests. The results are reported in Fig. 8.

This behaviour can be explained by analysing the mechanism of H_2 formation occurring in a PECa cell, as schematized in Fig. 9.

In the PECa approach, differently from the previous case (gas-phase GPR reactor), the electrons and protons generated on the photo-anode should be transported on the other side (dark) of the PECa cell, to be used by the electrocatalyst (in this case to generate H_2 in a separated compartment from that where O_2 formation occurs by water oxidation). The presence of vertically aligned TNT arrays is necessary, in addition to the plasmonic–photonic synergetic effects discussed before, to improve the transport of electrons and protons (produce from water photo-oxidation) from the top of the tubes to the bottom part to be collected from the Ti porous layer (to be transferred through the external circuit to the cathode side) or to be transferred to the cathode side via the H^+-conductive membrane (Nafion-type). As electrocathode, Pt NPs on carbon support were used.

When non-modified TNT arrays are used in the PECa cell, ~195 µmol of hydrogen were measured in the cathode side after five-hour time of irradiation, while no H_2 was detected in the anode part. This is an excellent result if compared to the ~92 µmol of hydrogen obtained in the GPR reactor for ethanol dehydrogenation. If ethanol is added to the photo-anode, H_2 productivity increased even to ~355 µmol, evidencing the importance of having a PECa design with a separation of oxidation and reduction reactions. This indicates that even if further resistance related to charge transport are introduced in the PECa reactor scheme, with respect to the short-circuit type scheme present in the GPR reactor approach, the back reactions between the products of oxidation and reduction (O_2 and H_2) play a relevant role in determining the overall performances.

In presence of Au NPs on TNT surface, instead, the quantity of H_2 at the cathode decreased to ~93 µmol, but hydrogen was also formed at the photo-anode. This phenomenon is because part of the photo-generated current was short-circuited towards the Au NPs, which act as cathodic centres for the reduction reaction, as they behave during the tests in GPR reactor.

Fig. 10 shows data of H_2 evolution when the filter AM 1.5 G was used to simulate the solar spectrum.

While the order of productivity is the same with respect to the tests at open spectrum reported in Fig. 8, some considerations should be done about the ratio of AM1.5 G/open spectrum values for the different photo-catalysts. This ratio is ~16% for the non-modified TNT arrays by water photo-electrolysis and increases to ~18% in presence of Au NPs, as gold improves light absorption in the visible region. The percentages increase in presence of ethanol, becoming ~21% and ~ 25% for the non-and Au-modified TNT arrays, respectively. From a thermodynamic point of view, water splitting is less favourable than ethanol dehydrogenation, thus H_2 formation is energetically more difficult when visible light is used.

3.4. PECa efficiency

In the case of PECa cells involving semiconductors, the three major processes leading to water splitting and influencing the overall photoconversion efficiency are: (i) the absorption of

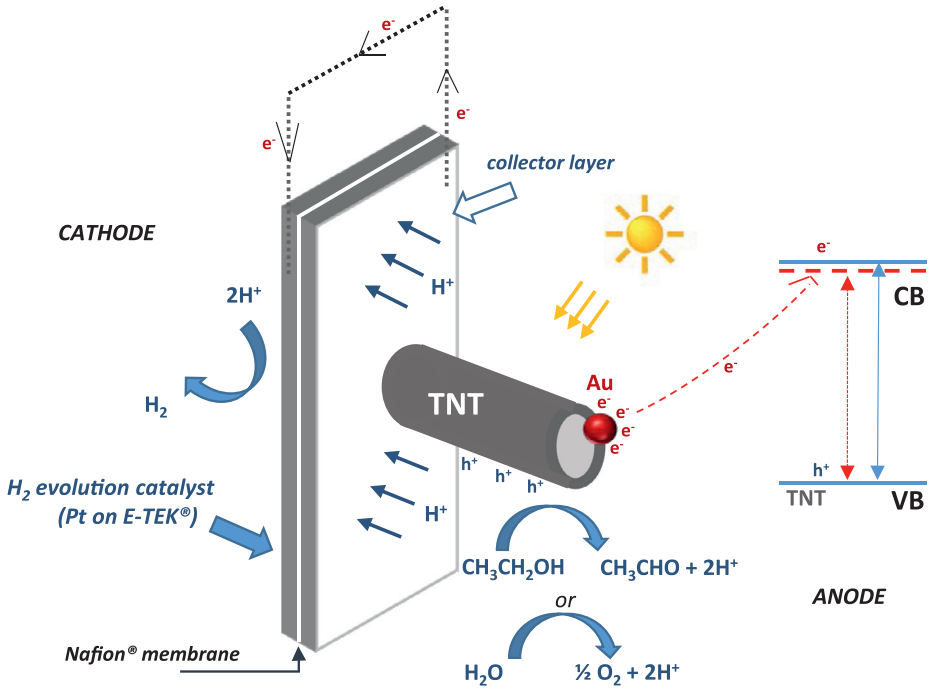

Fig. 9. Schematic mechanism of water photo-electrolysis and/or ethanol photo-dehydrogenation over Au-modified TNT arrays as photo-anode in a PECa cell with separation of oxidation and reduction zones.

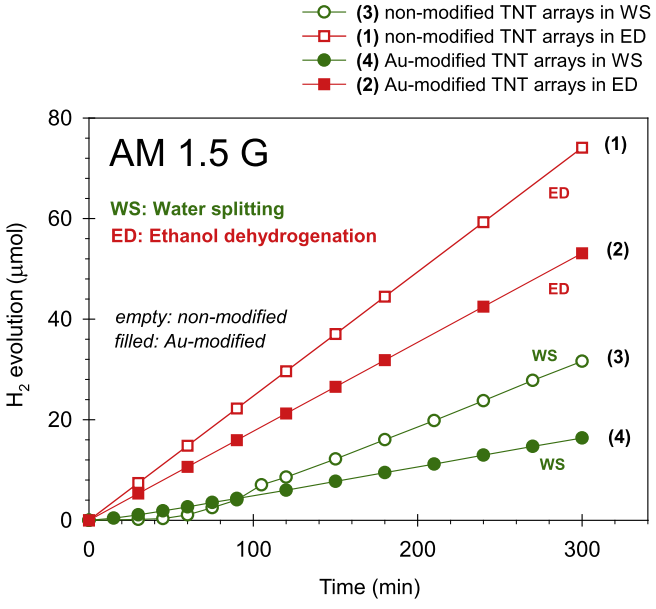

Fig. 10. Hydrogen evolution as a function of time from the cathode of a PECa cell in water splitting (WS) and ethanol dehydrogenation (ED). AM 1.5 G filter was used to filter the incident light.

photons having sufficient energy to equal or exceed the band gap of the semiconductor, (ii) the conversion of absorbed photons into separated charges and (iii) the utilization of these charges for water splitting and/or ethanol photo-reforming. Although the knowledge of the efficiency of each individual process would be required to evaluate the different aspects of PECa performance, the evaluation of the global photoconversion efficiency (called solar-to-hydrogen efficiency, if solar energy is used) is of great importance, especially for practical application. There are several approaches to calculate the overall photoconversion efficiency. In general, it is defined as the ratio between the maximum energy output that can be obtained from the final products (hydrogen or oxygen) and the energy supplied (in the form of light energy) [57]. For the experimental tests performed in PECa cell over non- and Au-modified TNT arrays, the solar-to-hydrogen (STH) efficiency was calculated by the formula:

$$\mathrm{STH} = \frac{R_{H2} \times \Delta G^0}{P_{tot} \times \mathrm{Area}} \quad (1)$$

where R_{H2} is the rate of hydrogen production (mol/s), ΔG^0 is the standard Gibbs energy at standard conditions (2.372×10^6 J/mol), P_{tot} is the irradiance from the illumination. Table 1 summarizes the STH values for the Au-modified TNT arrays prepared by electrodeposition in comparison with the non-modified TNT sample for both the processes of water photoelectrolysis and ethanol photo-dehydrogenation.

The maximum value of STH efficiency in absence of sacrificial reagents (water photo-electrolysis) was obtained for the non-modified TNT sample (0.83%). It is difficult to make comparison with other results reported in literature, as PECa systems are very different in terms of materials, configuration, and operating conditions, as well as different expressions are generally used for efficiency calculation. For instance, Xu et al. [27] recently published a paper on performance of 3D porous RGO-TiO_2 as photoanode for solar water splitting. They reported a STH conversion efficiency of 0.5% without the need of any sacrificial reagents under full-spectrum light irradiation, but they operated at low bias of 0.6 V (vs. Ag/AgCl), which was the potential showing the maximum of STH efficiency. Our results, instead, were obtained in a two-electrode configuration PECa cell without applying any bias between the electrodes ($V = 0$). Kargar et al. [58] reported an evaluation of PECa tandem cell performance using TiO_2/TiO_2 core/shell nanotube array as photoanode for overall solar water splitting. They calculated a STH of 0.18% using AM 1.5 G filter, against 0.23% obtained with our PECa cell.

Contrary to the experiments performed in gas phase (GPR) in which H_2 production was higher in presence of Au NPs,

Table 1. Solar-to-hydrogen (STH) efficiency for non- and Au-modified TNT arrays in PECa cell.

Process	Sample	STH (%)	Filter
Water photoelectrolysis	Non-modified TNT arrays	0.83	Open spectrum
	Non-modified TNT arrays	0.23	AM 1.5 G
	Au-modified TNT arrays	0.39	Open spectrum
	Au-modified TNT arrays	0.11	AM 1.5 G
Ethanol photo-dehydrogenation	Non-modified TNT arrays	1.43	Open spectrum
	Non- modified TNT arrays	0.24	AM 1.5 G
	Au- modified TNT arrays	0.93	Open spectrum
	Au- modified TNT arrays	0.20	AM 1.5 G

Table 2. Faradaic efficiency (η) for non- and Au-modified TNT arrays in PECa cell by water photo-electrolysis.

Sample	η (%)	Filter
Non-modified TNT arrays	61	Open spectrum
Non-modified TNT arrays	50	AM 1.5 G
Au-modified TNT arrays	91	Open spectrum
Au-modified TNT arrays	56	AM 1.5 G

the results obtained in the PECa system (with separation of oxidation/reduction zones) showed higher performance for the non-modified TNT sample, in terms of both H_2 production and STH efficiency. This phenomenon can be explained by the fact that the photo-generated current was partially short-circuited towards the Au NPs, which are deposited on the TNT electrode surface in the anodic side. Thus, part of the electric current was not collected and transferred to the cathodic side, but it was lost in the anode. This hypothesis is confirmed by the evolution of hydrogen also in the photo-anode, which we were able to detect only if Au NPs were deposited on the TNT surface. In this case, the mechanism is similar to that described in Fig. 6 for the gas-phase, with the Au NPs acting as cathodic centres for the reduction reaction. It is to notice that STH efficiency values referring to Au-modified TNT samples were calculated by taking into account only H_2 production rate from the cathode side, but performance increases if STH efficiency calculation also includes H_2 formation at the anode side.

Moreover, Faradaic efficiency was evaluated for testing experiments in water photo-electrolysis. The Faradaic efficiency (η) can be defined as the ratio between the effective and theoretical H_2 production rates:

$$\eta = \frac{H_2^{\text{meas}}}{H_2^{\text{theor}}} \quad (2)$$

where ${H_2}^{\text{meas}}$ is the measured H_2 production rate and ${H_2}^{\text{theor}}$ is the theoretical H_2 production rate estimated as:

$$H_2^{\text{theor}} = \frac{I \times t}{nF} \quad (3)$$

Where I is the generated photo-current during the PECa test, t the irradiation time, n the number of electrons involved in water splitting and F the Faradaic constant. Table 2 shows the η values for the Au-modified TNT arrays prepared by electrodeposition in comparison with the non-modified TNT sample for the process of water photo-electrolysis. All these values closed within 5% of error determination.

Notwithstanding STH efficiency is higher for the non-modified TNT arrays, due to less H_2 production rate for Au-modified TNT samples at the cathode side, Faradaic efficiency is higher when gold is present, especially for tests performed at open spectrum. This is to ascribe to the reduced charge recombination phenomena (in TNT lattice) when Au NPs are present on the top surface of the tubes. This effect is more evident at open spectrum, as the charge recombination between electrons and holes mainly refers to the conduction and valence bands of titania, working better if irradiated in the ultraviolet region.

4. Conclusions

In this work, different aspects about the behaviour of photo-electrocatalytic (PECa) devices for sustainable H_2 production were analysed. Discussion has mainly been centred on the evaluation of the factors that can control PECa performance and efficiency, through the analysis of results obtained over Au-modified TNT arrays.

The samples were prepared by controlled anodic oxidation of Ti foils and then doped with gold by using three different deposition techniques: wet impregnation, photo-reduction and electrodeposition. Particularly, electrodeposition consisted of multiple cycles of voltage ramps in presence of an aqueous solution containing the gold precursor salt, followed by a selective washing treatment.

Characterization data of Au-modified TNT arrays prepared by electrodeposition evidenced: (i) small Au NPs (3–5 nm) well dispersed on the top of highly ordered TNT arrays; (ii) a broad peak in the visible region due to both structural and surface plasmon resonance (SPR) effects; (iii) a slight shift of band gap towards the visible region with respect to non-modified TNT arrays; (iv) the presence of interference fringes in UV–visible spectrum. The synergy effect between nanotubular structures of TiO_2 and uniformly dispersed Au NPs, as well as the synergy between plasmonic–photonic effects (which depend on the method of gold deposition) allow to obtain good performance in terms of photo-generated current and H_2 production. Among the techniques investigated to deposit gold in TNTs, electrodeposition method allowed enhancing the photocurrent response, being 1.6 times higher than the photocurrent obtained from the non-modified TNT arrays. In gas-phase tests of ethanol photo-reforming, hydrogen production rate was also the highest for Au-modified TNT arrays with Au deposited by electrodeposition.

When a PECa approach was adopted, by separating the oxidation and reduction reactions, the results were analysed as hydrogen production rate, solar-to-hydrogen efficiency (STH) and Faradaic efficiency (η) that, from a practical point of view, are the most important factors for future industrial application. A STH efficiency of 0.83% was reached without adding any sacrificial reagent with non-modified TNT arrays, while the maximum η efficiency of 91% was obtained for the Au-modified TNT arrays. However, the effect of Au doping is unfavourable in terms of STH efficiency both in water photo-electrolysis and ethanol dehydrogenation, as the electric current (generated from the light absorption) is partially short-circuited at the photo-anode without the possibility to be converted into chemical energy (H_2) at the cathode side.

These results well evidenced how PECa performance and efficiency depend not only on the properties of the photo-active materials, but also on the design of the PECa device in which the catalysts are tested. We have not discussed here the characteristics of the electrocatalysts located in the cathodic (dark) side of the PECa cell, but also in this case an optimal design (for example, based on the use of carbon materials having a well-defined and controlled nano-scale dimension and functional properties) have to be utilized to maximize the production of solar fuels [59].

Acknowledgments

The TERRA (Tandem Electrocatalytic Reactor for energy/Resource efficiency and process intensification, H2020 project 677471) and Eco^{2}CO$_2$ (Eco-friendly biorefinery fine chemicals from CO_2 photo-catalytic reduction, FP7 project 309701) in the frame of which part of these studies reported here have been realized, are kindly acknowledged.

References

[1] N. Armaroli, V. Balzani, Chem. Eur. J. 22 (1) (2016) 32–57.
[2] S.-F. Leung, Q. Zhang, M.M. Tavakoli, J. He, X. Mo, Z. Fan, Small 12 (19) (2016) 2536–2548.
[3] C. Ampelli, G. Centi, R. Passalacqua, S. Perathoner, Energy Environ. Sci. 3 (3) (2010) 292–301.
[4] C. Ampelli, S. Perathoner, G. Centi, Philos. Trans. R. Soc. A. 373 (20140177) (2015) 1–35.
[5] M.G Walter, E.L. Warren, J.R. McKone, S.W. Boettcher, Q. Mi, E.A. Santori, N.S. Lewis, Chem. Rev. 110 (11) (2010) 6446–6473.
[6] S. Perathoner, G. Centi, D. Su, ChemSusChem 9 (4) (2016) 345–357.
[7] S. Bensaid, G. Centi, E. Garrone, S. Perathoner, G. Saracco, ChemSusChem 5 (3) (2012) 500–521.
[8] C. Ampelli, G. Centi, R. Passalacqua, S. Perathoner, Catal. Today 259 (2016) 246–258.
[9] R. Passalacqua, S. Perathoner, G. Centi, Catal. Today 251 (2015) 121–131.
[10] W. Zhou, Q. Xie, Prog. Chem. 25 (12) (2013) 1989–1998.
[11] S. Hernández, G. Gerardi, K. Bejtka, A. Fina, N. Russo, Appl. Catal. B. 90 (2016) 66–74.
[12] I. Natali Sora, F. Fontana, R. Passalacqua, C. Ampelli, S. Perathoner, G. Centi, F. Parrino, L. Palmisano, Electrochimica Acta 109 (2013) 710–715.
[13] C.R. Lhermitte, B.M. Bartlett, AccountsChem. Res. 49 (2016) 1121–1129.
[14] D. Kang, T.W. Kim, S.R. Kubota, A.C. Cardiel, H.G. Cha, K.-S. Choi, Chem. Rev. 115 (23) (2015) 12839–12887.
[15] X. Yang, R. Liu, Y. He, J. Thorne, Z. Zheng, D. Wang, Nano Res. 8 (1) (2014) 56–81.
[16] T. Hisatomi, J. Kubota, K. Domen, Chem. Soc. Rev. 43 (22) (2014) 7520–7535.
[17] C. Ampelli, C. Genovese, G. Centi, R. Passalacqua, S. Perathoner, Top. Catal. 59 (8–9) (2016) 757–771.
[18] C. Wu, Z. Gao, S. Gao, Q. Wang, H. Xu, Z. Wang, B. Huang, Y. Dai, J. Energy Chem. 25 (4) (2016) 726–733.
[19] C. Hu, C. Lian, S. Zheng, X. Li, T. Lu, Q. Hu, S. Duo, R. Zhang, Y. Sun, F. Chen, J. Energy Chem. 25 (3) (2016) 489–494.
[20] G. Zhang, H. Miao, X. Hu, J. Mu, X. Liu, T. Han, J. Fan, E. Liu, Y. Yin, J. Wan, Appl. Surf. Sci. 391 (2017) 345–352.
[21] V.R. Subramanian, R.D. Braatz, Electrochem. Soc. Interface 19 (2) (2010) 37–38.
[22] M.A. Modestino, S.M.H. Hashemi, S. Haussener, Energy Environ. Sci. 9 (5) (2016) 1533–1551.
[23] C. Ampelli, R. Passalacqua, S. Perathoner, G. Centi, Chem. Eng. Trans. 17 (2009) 1011–1016.
[24] C. Ampelli, C. Genovese, R. Passalacqua, S. Perathoner, G. Centi, Theor. Found. Chem. Eng. 46 (6) (2012) 651–657.
[25] D. Kopljar, A. Inan, P. Vindayer, N. Wagner, E. Klemm, J Appl. Electrochem. 44 (10) (2014) 1107–1116.
[26] C. Genovese, C. Ampelli, S. Perathoner, G. Centi, J. Energy Chem. 22 (2) (2013) 202–213.
[27] X. Xu, B. Feng, G. Zhou, Z. Bao, J. Hu, Mater. Design 101 (2016) 95–101.
[28] K. Ueno, T. Oshikiri, H. Misawa, ChemPhysChem 17 (2) (2016) 199–215.
[29] P. Zhang, T. Wang, J. Gong, Adv. Mater. 27 (36) (2015) 5328–5342.
[30] N. Zhou, V. López-Puente, Q. Wang, L. Polavarapu, I. Pastoriza-Santos, Q.-H. Xu, RSC Adv. 5 (37) (2015) 29076–29097.
[31] A.M. Qureshy, M. Ahmed, I. Dincer, Int. J. Hydrog. Energy 41 (19) (2016) 8020–8031.
[32] C.-J. Tseng, C.-L. Tseng, Int. J. Hydrog. Energy 36 (11) (2011) 6510–6518.
[33] Z. Xing, X. Zong, J. Pan, L. Wang, Chem. Eng. Sci. 104 (2013) 125–146.
[34] Y.L. Pang, S. Lim, H.C. Ong, W.T. Chong, Appl. Catal. A Gen. 481 (2014) 127–142.
[35] Mor G.K, O.K. Varghese, M. Paulose, K. Shankar, C.A. Grimes, Sol. Energy Mater. Sol. Cells 90 (14) (2006) 2011–2075.
[36] J.M. Macak, H. Tsuchiya, A. Ghicov, K. Yasuda, R. Hahn, S. Bauer, P. Schmuki, Curr. Opin. Solid State Mater. Sci. 11 (1–2) (2008) 3–18.
[37] R. Passalacqua, C. Ampelli, S. Perathoner, G. Centi, Nanosci. Nanotechnol. Lett. 4 (2) (2012) 142–148.
[38] C. Ampelli, R. Passalacqua, S. Perathoner, G. Centi, D.S. Su, G. Weinberg, Top. Catal. 50 (1–4) (2008) 133–144.
[39] C. Ampelli, C. Genovese, B.C. Marepally, G. Papanikolaou, S. Perathoner, G. Centi, Faraday Discuss. 183 (2015) 125–145.
[40] C. Ampelli, C. Genovese, M. Errahali, G. Gatti, L. Marchese, S. Perathoner, G. Centi, J. Appl. Electrochem. 45 (7) (2015) 701–713.
[41] C. Genovese, C. Ampelli, S. Perathoner, G. Centi, J. Catal. 308 (2013) 237–249.
[42] C. Ampelli, C. Genovese, F. Tavella, M. Favaro, S. Agnoli, G. Granozzi, S. Perathoner, G. Centi, Chem. Eng. Trans. 43 (2015) 667–672.
[43] C. Ampelli, C. Genovese, R. Passalacqua, S. Perathoner, G. Centi, Appl. Therm. Eng. 70 (2) (2014) 1270–1275.
[44] C. Ampelli, R. Passalacqua, C. Genovese, S. Perathoner, G. Centi, T. Montini, V. Gombac, J.J. Delgado, P. Fornasiero, RSC Adv. 3 (44) (2013) 21776–21788.
[45] C. Ampelli, R. Passalacqua, S. Perathoner, G. Centi, Chem. Eng. Trans. 24 (2011) 187–192.
[46] C. Ampelli, F. Tavella, S. Perathoner, G. Centi, Chem. Eng. J. (2016) submitted.
[47] Y. Tian, T. Tatsuma, J. Am. Chem. Soc. 127 (20) (2005) 7632–7637.
[48] R. Reichert, Z. Jusys, R.J. Behm, J. Phys. Chem. C 119 (44) (2015) 24750–24759.
[49] P. Li, S.-L. Chen, A.-J. Wang, Y. Wang, Chem. Eng. J. 284 (2016) 305–314.
[50] G. Centi, R. Passalacqua, S. Perathoner, D.S. Su, G. Weinberg, R. Schlögl, Phys. Chem. Chem. Phys. 9 (35) (2007) 4930–4938.
[51] Z. Zhang, L. Zhang, M.N. Hedhili, H. Zhang, P. Wang, Nano Lett. 13 (1) (2013) 14–20.
[52] B.Y. Zheng, H. Zhao, A. Manjavacas, M. McClain, P. Nordlander, N.J. Halas, Nat. Commun. 6 (2015) 7797.
[53] C. Clavero, Nat. Photonics. 8 (2) (2014) 95–103.
[54] A. Sousa-Castillo, M. Comesanã-Hermo, B. Rodríguez-González, M. Pérez-Lorenzo, Z. Wang, X.-T. Kong, A.O. Govorov, M.A. Correa-Duarte, J. Phys. Chem. C 120 (21) (2016) 11690–11699.
[55] Z. Cai, Z. Xiong, X. Lu, J. Teng, J. Mater. Chem. A 2 (2) (2014) 545–553.
[56] S.K. Jana, T. Majumder, S. Banerjee, J. Electroanal. Chem. 727 (2014) 99–103.
[57] O.K. Varghese, C.A. Grimes, Sol. Energy Mater. Sol. Cells 92 (4) (2008) 374–384.
[58] A. Kargar, J. Khamwannah, C.-H. Liu, N. Park, D. Wang, S. Dayeh, S. Jin, Nano Energy 19 (2016) 289–296.
[59] C. Ampelli, S. Perathoner, G. Centi, Chin. J. Catal. (CuihuaXuebao) 35 (6) (2014) 783–791.